Design and Synthesis of Aviram-Ratner-Type Dyads and Rectification Studies in Langmuir-Blodgett (LB) Films

Govindasamy Jayamurugan,[a] Vijayendran Gowri,[a] David Hernández,[b] Santiago Martin,[b, c] Cagatay Dengiz,[a] Francesc Pérez-Murano,[d] Jean-Paul Gisselbrecht,[e] Corinne Boudon,[e] W. Bernd Schweizer,[a] Benjamin Breiten,[a] Aaron D. Finke,[a] Gunnar Jeschke,[f] Bruno Bernet,[a] Laurent Ruhlmann,[e] Pilar Cea,*[b, g] and François Diederich*[a]

[a] *Dr. G. Jayamurugan, Dr. V. Gowri, C. Dengiz, Dr. W. B. Schweizer, Dr. B. Breiten, Dr. A. D. Finke, Dr. B. Bernet, Prof. Dr. F. Diederich,*
Laboratorium für Organische Chemie, ETH Zurich
Vladimir-Prelog-Weg 3, CH-8093 Zurich, Switzerland
Fax: (+41) 44 632 1109
E-mail: diederich@org.chem.ethz.ch

[b] *D. Hernández, Prof. Dr. S. Martin, Prof. Dr. P. Cea*
Departamento de Química Física, Facultad de Ciencias
Universidad de Zaragoza, 50009 Zaragoza, Spain
Fax: (+34) 976 761 202
E-mail: pilarcea@unizar.es

[c] *Prof. Dr. S. Martin*
Instituto de Ciencia de Materiales de Aragón (ICMA)
Universidad de Zaragoza-CSIC, 50009 Zaragoza, Spain

[d] *Prof. Dr. F. Perez-Murano*

Instituto de Microelectrónica de Barcelona (IMB-CNM, CSIC), Campus UAB, 08193 Bellaterra, Spain

[e] *Dr. J.-P. Gisselbrecht, Prof. Dr. C. Boudon, Prof. Dr. L. Ruhlmann*

Laboratoire d'Electrochimie et de Chimie Physique du Corps Solide, Institut de Chimie-UMR 7177, C.N.R.S., Université de Strasbourg, 4 rue Blaise Pascal, CS 90032, 67081 Strasbourg Cedex, France

[f] *Prof. Dr. G. Jeschke*

Laboratory of Physical Chemistry, ETH Zurich

Vladimir-Prelog-Weg 2, CH-8093 Zurich, Switzerland

[g] *Prof. Dr. P. Cea*

Instituto de Nanociencia de Aragón (INA) and Laboratorio de Microscopias Avanzadas (LMA), Edificio i+d. Campus Rio Ebro Universidad de Zaragoza, C/Mariano Esquillor, s/n, 50017 Zaragoza, Spain

Supporting Information (SI) for this article is available on the WWW under xxxx

Abstract: The design and synthesis of Aviram-Ratner-type molecular rectifiers, featuring an anilino-substituted extended tetracyanoquinodimethane (exTCNQ) acceptor, covalently linked by the σ-spacer bicyclo[2.2.2]octane (BCO) to a tetrathiafulvalene (TTF) donor moiety, are described. The rigid BCO spacer keeps the TTF donor and exTCNQ acceptor moieties apart, as demonstrated by X-ray analysis. The photophysical properties of the TTF-BCO-exTCNQ dyads were investigated by UV/Vis and EPR spectroscopy, electrochemical studies, and theoretical calculations. Langmuir-Blodgett films were prepared and used in the fabrication and electrical studies of junction devices. One dyad showed the asymmetric current-voltage (*I-V*)

curve characteristic for rectification, unlike a control compound lacking the donor TTF part which gave a symmetric *I-V* curve. The direction of the observed rectification indicated that the preferred electron current flows from the exTCNQ acceptor to the TTF donor.

Keywords: Aviram–Ratner dyad • Langmuir-Blodgett films • rectification • charge-transfer • [2+2] cycloaddition–retroelectrocyclization (CA–RE) • molecular electronics materials

Introduction

In 1974, Aviram and Ratner developed the concept of a "molecular rectifier", a single organic molecule showing unidirectional electron flow in an applied field.[1] Their molecular design criteria for rectification behavior are simple: a dyad consisting of an electron-rich "π-donor" (D) and an electron-poor "π-acceptor" (A) which are separated by a rigid, insulating "spacer" (σ). The originally proposed dyad **1** (Figure 1) has been theoretically proven to be an effective candidate for an organic molecular rectifier,[1] but in view of synthetic complexity, has not been reported to date.[2]

However, **1** is not alone in its potential to display rectification behavior and several groups have since followed the Aviram–Ratner design criteria to find new leads for molecular rectifiers with D-σ-A architectures.[3] The synthetic challenges are considerable. The donor and acceptor need to be sufficiently strong to have high-lying HOMOs and low-lying LUMOs, respectively, but without undergoing spontaneous redox chemistry. The insulating spacer needs to be rigid and long enough to efficiently inhibit intramolecular charge-transfer (CT). Only a few dyads have been reported to overcome these challenges and to display rectification behavior.[3a,3e,3r]

While dyads featuring tetrathiafulvalene (TTF) as donor and 7,7,8,8-tetracyano-*p*-quinodimethane (TCNQ) or other strong acceptors have been prepared, the rigid σ-spacer required by the Aviram-Ratner proposal has so far not been realized. Flexible spacers have prevented rectification behavior by leading to thermal electron transfer in the ground state[4] or intramolecular CT.[5]

Here, we report the synthesis and properties of the two new dyads **2** and **3** (Figure 1) featuring for the first time all three main components of the original Aviram-Ratner design, with a TTF donor separated by a bicyclo[2.2.2]octane (BCO) spacer from a donor-substituted extended TCNQ (exTCNQ) acceptor moiety. We show rectification behavior for **3** in Langmuir-Blodgett films.

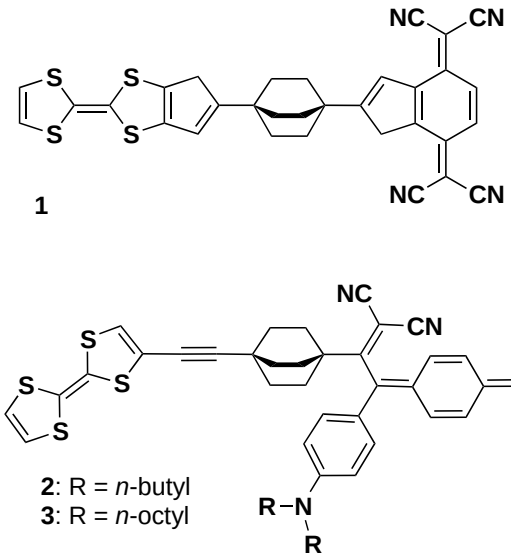

Figure 1: Top: Original molecular rectifier **1** proposed by Aviram and Ratner.[1] Bottom: D-σ-A dyads **2** and **3** featuring all three key elements of the original proposal.

Results and Discussion

Synthesis and characterization of D-σ-A dyads 2 and 3.

The preparation of dyad **3** is shown in Scheme 1 whereas the synthesis of dyad **2** is described in Scheme S1 in the Supporting Information (SI). We chose a synthetic

strategy that allows for late-stage generation of the anilino-substituted exTCNQ acceptor moiety, using the [2+2] cycloaddition–retroelectrocyclization (CA–RE) cascade reaction between aniline donor-activated alkyne and TCNQ.[6,7]

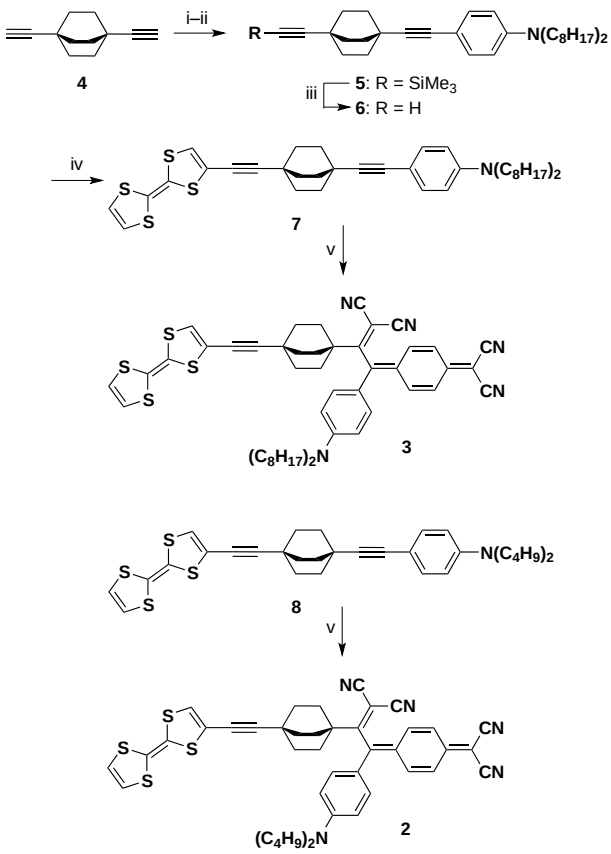

Scheme 1: Synthesis of dyads **2** and **3**. i) *n*-BuLi, Me_3SiCl, Et_2O, –78 °C, 1 h; ii) *N*,*N*-dioctyl-4-iodoaniline, $[PdCl_2(PPh_3)_2]$, CuI, Et_3N, 20 °C, 12 h, 35% (over two steps); iii) K_2CO_3, MeOH, 25 °C, 2.5 h, 98%; iv) 2-Iodo-TTF, $[Pd(PPh_3)_4]$, CuI, benzene/Et_3N, 60 °C, 15 h, 40%; v) TCNQ, $(CHCl_2)_2$, 120 °C, 2.5 h, 75% (**3**), 70% (**2**).

The synthesis of **3** started from 1,4-diethynylbicyclo[2.2.2]octane (**4**)[8] which was mono-silyl protected and transformed by Sonogashira cross-coupling with *N*,*N*-dioctyl-4-iodoaniline[9] into compound **5**. Silyl-deprotection afforded **6** which was

cross-coupled with 2-iodo-TTF[10] to give dyad precursor **7**. Precursor **8** to dyad **2** was obtained by a similar reaction sequence (Scheme 1; see Scheme S1 in the SI).

The generation of the exTCNQ moiety by the CA–RE reaction was first attempted by treating TCNQ with precursor **8** at room temperature. However, TCNQ did not undergo the CA–RE reaction with **8** at 25 °C; instead, an intense color change was observed from brownish yellow to green, due to the formation of an 1:1 intermolecular charge-transfer complex, presumably with the TTF moiety. To overcome this, we adopted a TTF oxidation-masking approach developed by Stoddart and co-workers.[11] Oxidation of the TTF moiety of **8** with $Fe(ClO_4)_2 \cdot 2\ H_2O$ in MeCN allowed TCNQ to react with the anilino donor-activated alkyne moiety at room temperature; subsequent reduction of the oxidized TTF with sodium L-ascorbate in MeOH gave dyad **2** in 40% isolated yield. Later, we found that this approach was unnecessary; simply heating **8** or **7** with TCNQ to 120 °C in $(CHCl_2)_2$ for 2.5 h gave dyads **2** and **3**, respectively, in 70–75% yield (Scheme 1). Notably, the TTF donor-activated alkyne moiety did not react with TCNQ[12] and only the anilino-activated alkyne moiety underwent the CA–RE reaction, as this regiochemistry was confirmed by single crystal X-ray diffraction of dyad **2** (Figure 2, also see the SI, Section B). The two dyads are stable, maroon-colored metallic solids, giving green solutions in CH_2Cl_2. They melt at 226–230 °C (**2**) and at 109–110 °C (**3**).

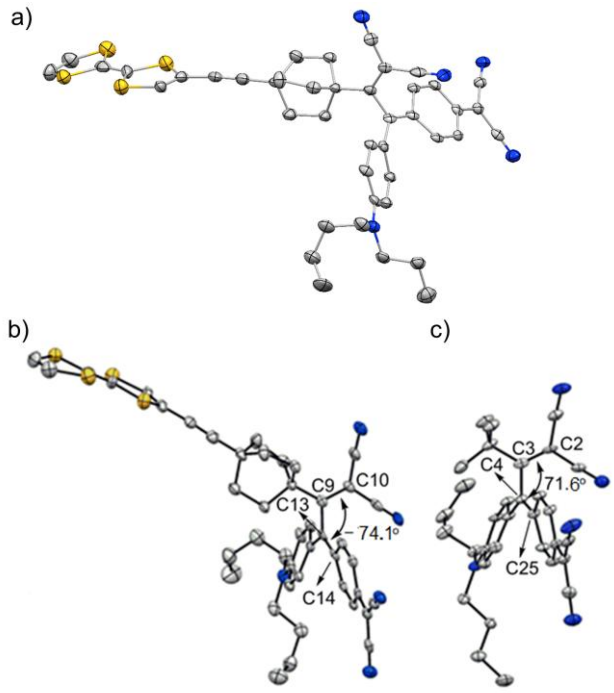

Figure 2: Crystal structures of **2** (a,b) and **9** (c) at 100 K. H-atoms for **2** and **9** and solvent molecules for **2** are omitted for clarity. Atomic displacement parameters are drawn at 50% probability level. Some carbon atoms are labeled with arbitrary numbering.

Figure 3 shows important control compounds **9** and **10** containing only the aniline-substituted exTCNQ acceptor moiety and compound **11** as a reference for the donor part. Their synthesis is shown in Scheme S2 in the SI. X-ray analysis of **9** revealed that the conformation around the single bond located between the dicyanovinyl group and the 2-(4-methylene-2,5-dien-1-ylidene)malononitrile group is similar to that observed for dyad **2** (torsional angle C2-C3-C4-C25 of 71.6(4)° for **9** and C10-C9-C13-C14 of 74.1(6)° for **2**; Figure 2).

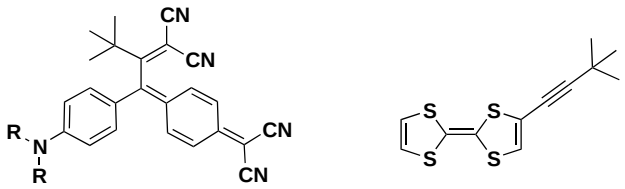

9: R = *n*-butyl
10: R = *n*-octyl

11

Figure 3: Control compounds **9**-**11**.

Electronic absorption spectra

The UV/Vis absorption spectra of dyads **2**, **3** and reference compounds **9**–**11** are shown in Figure 4, in order to obtain information about the nature and origin of the CT interactions, which may occur between the donor (dialkylanilino (DAA) and TTF moieties) and the acceptor (exTCNQ) moieties in either inter- or intramolecular fashion.

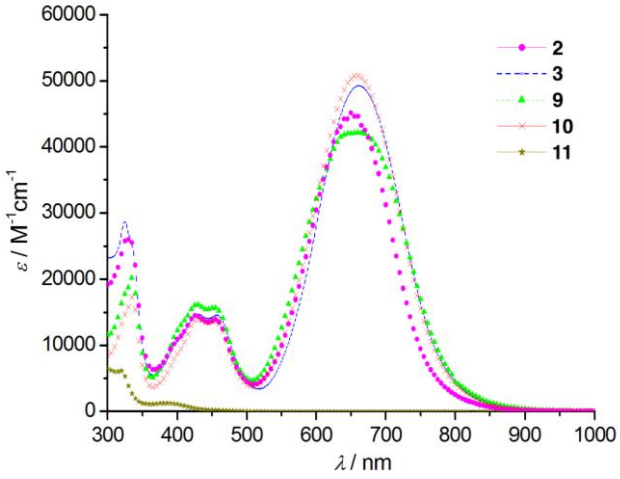

Figure 4: UV/Vis absorption spectra of dyads **2**, **3** and reference compounds **9**-**11** in CH_2Cl_2 at 298 K.

Dyads **2**, **3** and reference compounds **9**, **10** feature a very similar strong low-energy absorption band at around 660 nm. This band is therefore clearly originating from the intramolecular CT between the DAA donor and the directly connected

exTCNQ acceptor. The TTF reference compound **11** has no absorption above 450 nm. The spectral data indicate that the TTF donor and the exTCNQ acceptor moieties are not interacting in the ground state. The proposed intramolecular CT character of the longest-wavelength absorption bands of dyads **2**, **3** and reference compounds **9**, **10** was confirmed by protonation of the aniline donor moiety. Treatment of these compounds with CF_3COOH in CH_2Cl_2 led to disappearance of the CT band (see Figures S3 and S4), with reappearance of the band upon re-neutralization with NEt_3. However, it should be noted that under acidic conditions, a new weaker band appears at around 640 nm in both dyads **2** and **3** (Figure S3), but not in the case of the reference compounds **9** and **10** indicating that this band is possibly due to partial protonation/oxidation of the TTF moiety.[13]

Dyads **2**, **3** and reference compounds **9**, **10** display strong solvatochromic behavior. A remarkably large hypsochromic shift is observed from ~660 nm (1.89 eV) in CH_2Cl_2, to ~575 nm (2.16 eV) nm in hexane, owing to high electric transition dipole moments (see Figures S5–S6 in the SI). This pronounced solvatochromism is also reflected in the change of the color of **2** from green in CH_2Cl_2 to purple in hexane (see Figure S7 in the SI).

Electrochemistry

The redox properties of dyads **2**,**3** and reference compounds **9**–**11** were studied by cyclic voltammetry (CV) and rotating-disc voltammetry (RDV) in CH_2Cl_2 (+0.1 M nBu$_4$NPF$_6$, values reported vs. Fc^+/Fc) (see Table S1 in the SI).

Dyads **2** and **3** display one irreversible one-electron oxidation step of the DAA moiety at +0.42 and +0.45 V, respectively, and two reversible one-electron oxidation steps of the TTF moiety at +0.00 and ~+0.50 V; however, for **2** the second oxidation

is irreversible, possibly due to the poor solubility of the oxidized species. The dyads also exhibit reversible two-electron reduction steps at –0.90 V, centered on the exTCNQ acceptor. One two-electron reduction was also observed for references **9** and **10** at potentials similar to that of **2** and **3** (–0.90 V), suggesting that the reduction waves are not affected by the presence of the TTF donor.

The UV/Vis and electrochemical data are clear evidence that intramolecular CT of **2**, **3**, **9**, and **10** occurs intramolecularly from the DAA donor to the directly connected exTCNQ acceptor moiety. As predicted, the CT from the TTF moiety to the exTCNQ acceptor part is suppressed by the insulating BCO moiety. This finding was further corroborated by the electron paramagnetic resonance (EPR) spectral investigations. A negligible amount of EPR signal is observed for dyad **2**, with the intensity measured to be 0.02% against (2,2,6,6-tetramethyl-piperidin-1-yl)oxyl (TEMPO) as reference (see Figure S10 in the SI). This could be due to the inherent nature of the exTCNQ moiety as it has been reported that some polycyanobutadienes exhibit EPR signals.[6b,14] The vanishing amount of radical contamination is also reflected by the sharp signals in the ^{1}H and ^{13}C NMR spectra of **2** (Figures S17 and S18 in the SI). The above results confirm the almost complete absence of ground state CT between TTF donor and exTCNQ acceptor moieties, and individual molecules are present in neutral form in the ground state.

The spatial separation of the donor and acceptor orbitals in dyads **2** and **3** was further supported by computational methods. Geometry optimization and orbital visualization of **2** was performed by DFT calculations (B3LYP/G-61G*, Gaussian09; see the SI, Section F).[15] As expected, the HOMO is localized on the TTF donor, the LUMO and LUMO+1 on the exTCNQ acceptor, and the HOMO–1 on the aniline moiety. The electron affinity (*EA*) and ionization potential (*IP*) of **2** are in the range of

1–3.5 V and 5–9 V, respectively, favorable for achieving an asymmetry current flow governed by a rectifier.[3f] The optical gaps of **2**, **3**, **9**, and **10** were also calculated from the end-absorption λ_{end} of the longest-wavelength UV/Vis band. They correlate reasonably well (R^2 = 1.02) with the results $\Delta(E_{ox}–E_{red})$ of the electrochemical measurements, evidencing that the same orbitals are involved in both optical and electrochemical gaps (Table 1).

Table 1. Optical and electrochemical gaps of **2**, **3**, **9**, and **10** determined by UV/Vis spectroscopy and CV in CH_2Cl_2.

Compound	λ_{max} [nm (eV)]	λ_{end} [nm (eV)]	$\Delta(E_{ox}–E_{red})$ [V]	$E_{1/2}$ [V]
2	650 (1.91)	890 (1.39)	1.32	+0.42,[a] –0.90
3	660 (1.88)	910 (1.36)	1.35	+0.45,[a] –0.90
9	660 (1.88)	900 (1.38)	1.35	+0.43,[a] –0.92
10	660 (1.88)	900 (1.38)	1.39	+0.43,[a] –0.96

[a] Irreversible peak potential. The electrochemical gaps were listed for the DAA donor oxidation and the exTCNQ acceptor reduction values.

The estimated electrochemical gaps of **2** and **3** (0.90 V; calculated from the TTF donor oxidation and the exTCNQ acceptor reduction potentials) and their electron affinities (ΔE_{LUMO}; 2.35 V) (Figure 5) encouraged us to apply the TTF-BCO-exTCNQ dyads to monolayer and rectification studies.

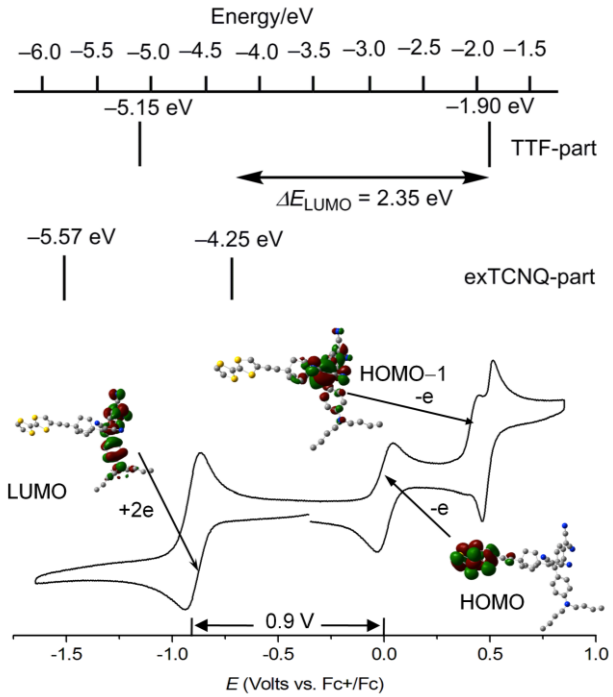

Figure 5: Top: HOMO of the TTF donor and LUMO of the exTCNQ acceptor parts of **2** and **3**. Bottom: Cyclic voltammogram of **3** with the corresponding HOMO and LUMO pictures of **2**.

Preparation and characterization of LB monolayers of TTF-BCO-exTCNQ dyads.

Dyads **2** and **3** were assembled by the LB technique.[16] Figure 6 shows the representative surface pressure (π-A) isotherms of **2** and **3**. The π-A isotherm of **3** is significantly more expanded suggesting a lower molecular aggregation during the compression process. Changes in the slope upon the compression process reveal a progressive orientation and/or reorientation of the molecules at the interface. Brewster angle microscopy (BAM) investigations[17] were made upon the compression of the Langmuir (L) film and gave further insight into the formation of the monolayers (see Section G, Figure S11 in the SI). BAM images indicate significant differences between the two monolayers. Non-homogeneous domains were observed for **2**, while

a very homogeneous and compact L film was detected for **3** in the compression process even at low surface pressures.

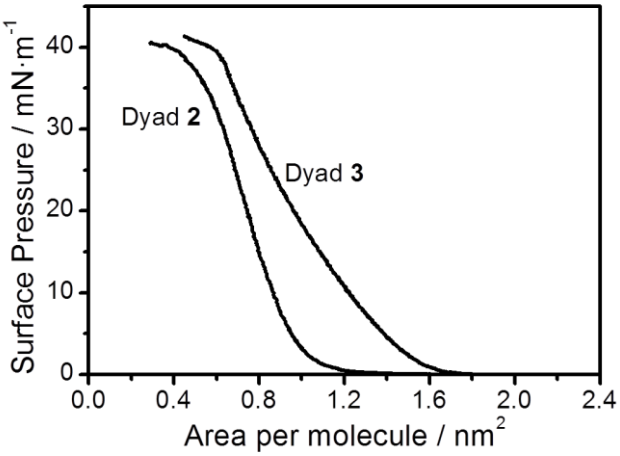

Figure 6: Surface pressure vs. area per molecule isotherms of dyads **2** and **3** on a water subphase at 20 ºC.

To confirm these observations, L monolayers of **2** and **3** were transferred onto freshly cleaved mica substrates to evaluate the morphology of the LB films by atomic force microscopy (AFM). AFM images of **2** and **3** at different surface pressures of transference are shown in Figure S12 in the SI, confirming that **3** transferred at 10 $mN{\cdot}m^{-1}$ forms homogeneous films free of holes or three-dimensional defects. The film thickness, 2.18 nm, was determined by scratching the film of dyad **3** transferred at 10 $mN{\cdot}m^{-1}$ with the AFM tip. This value is in excellent agreement to the length of the molecule (2.20 nm) determined with a molecular modelling program (Spartan®08 V 1.0.0).A further study was carried out to gain additional information about the molecular orientation in the LB films incorporating dyad **3**. L films of **3** were transferred onto quartz substrates at a surface pressure of 10 $mN{\cdot}m^{-1}$, and the UV/Vis absorption spectrum of the LB film was recorded (see Section G, Figure S13 in the SI). The differences in the wavelengths (both L and LB films show a ~5 nm

bathochromic shift of the ~320 nm band as well as a ~20 nm bathochromic shift of the ~650 nm band) between the solution in chloroform, the L film, and the LB film spectra are indicative of a different chemical environment of **3**, in agreement with the solvatochromism mentioned above. In addition, the UV/Vis spectrum of the dyad **3** in solution shows mainly two broad low energy absorption bands at ~650 nm and ~420 nm with the corresponding molar absorptivity ratio of 3:1, respectively (Figure S13). Whereas the UV/Vis spectra of the L and LB films of **3** showed significant change in the molar absorptivity ratios of 1:1 and 1:1.5, respectively. These resultsreveal molecular reorganizations during the transference process of the L film onto the substrate and a different relative orientation of these moieties in the L and LB films (see Figure S13 in the SI). The different molar absorptivities of the films with respect to the chloroform solution and cast films are also attributed to orientation effects.

XPS experiments were carried out in LB films of dyad **3** deposited onto gold substrates to obtain more information about the molecular orientation. Figure 7 shows the XPS scans of the S2p and N1s region in LB films transferred at a surface pressure of 10 $mN \cdot m^{-1}$; the XPS of dyad **3** powder and cast films of **3** are also included for comparison purposes. The XPS spectrum of a solid sample of **3** powder in the S2p region shows doublet peaks due to the spin-orbit splitting effect[9-11] at 164.0 and 165.2 eV, with an area ratio of 2:1 and a peak separation of 1.2 eV, corresponding to the ($2p_{3/2}$) and ($2p_{1/2}$) peaks. In contrast, the XPS spectrum of the LB film of **3** shows four peaks. Two of them appear practically at the same bonding energy to the ones observed for the powder and keep the same area ratio, 2:1, and peak separation of 1.2 eV revealing that part of the sulfur species do not interact with the gold substrate. However, a new doublet peak, also with a 2:1 area ratio and a peak separation of 1.2

eV, appears at 161.7 and 162.9 eV. This decrease in the binding energy has generally been interpreted as sulfur being adsorbed onto the gold surface.[12] These results indicate that part of the sulfur atoms are chemisorbed on the gold substrate. In contrast, the XPS spectrum of cast films (prepared from a diluted solution) exhibits only two peaks centered at 161.7 and 162.9 eV. This result indicates that in cast films molecules tend to adopt a planar position with all the sulfur atoms interacting with the gold surface.

The XPS spectrum of the LB film in the N1s region does not show any significant changes in the binding energy of the peaks (402.3 and 399.8 eV attributable to the amine and the cyano nitrogens, respectively) compared to the powder XPS spectrum indicating that there is no chemical interaction between the nitrogen species of dyad **3** and the gold substrate. However, there is a significant shift of these peaks towards lower binding energies in cast films. This result suggests that in cast films the nitrogen atoms of dyad **3** are chemisorbed on the gold surface.

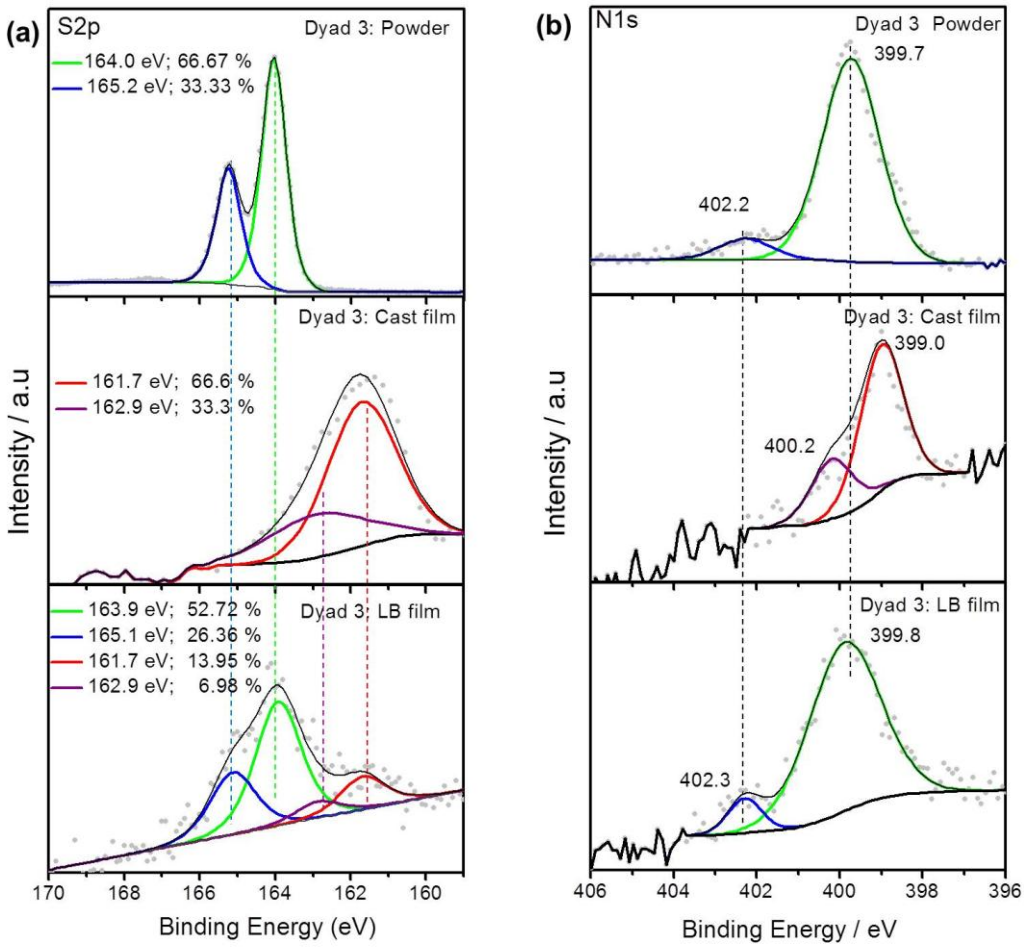

Figure 7. XPS spectra of (a) S2p and (b) N1s photoelectrons of dyad **3** in powder, in cast films, and in LB films transferred at 10 $mN \cdot m^{-1}$. In all cases the supporting substrate was gold.

Fabrication and electrical studies of junction devices with 3.

Rectification studies for LB films have been reported before.[3c,3h,3r,16b,18] Here, rectification studies of LB films incorporating dyad **3** were performed by making use of current-voltage (*I*-*V*) curves recorded with a conductive-AFM instrument. Further details about the experimental conditions and advantages of using the PF-TUNA™ operation mode for the AFM[19] are detailed in the Experimental Section. The

electrical behavior of LB films of reference compound **10** was also studied (details for the LB fabrication and electrical characterization of **10** are in Section G in the SI).

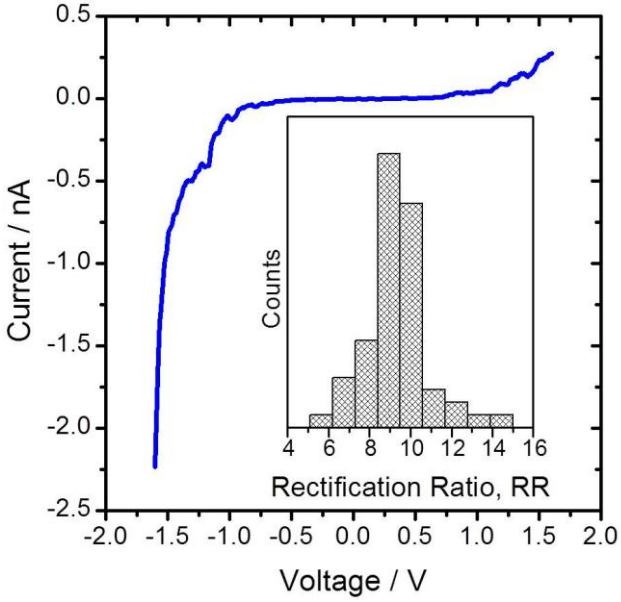

Figure 8: *I–V* curve of a monomolecular LB film of dyad **3** transferred onto Au(111) at 10 $mN \cdot m^{-1}$. Inset figure: statistical distribution of the rectification ratio obtained from 180 *I-V* curves.

Figure 8 shows an averaged *I-V* curve, from 180 *I-V* curves, for dyad **3** recorded using a peak force set-point of 65 nN. A compromise was made in order to select the most suitable contact force to be applied during the measurement. Thus, 65 nN was the minimum force needed for an adequate electrical probing and did not result in damage to the monolayer. Figure 8 shows a typical rectification behavior, since above a threshold voltage the current significantly decreases for negative voltages while at positive voltages the current hardly changes. Importantly, such a rectification behavior was not observed for reference compound **10**, that exhibits symmetric *I-V* curves (see Figure S15 in the SI). These results indicate that the rigid σ-spacer, not present between the aniline donor and exTCNQ acceptor moieties in **10**, is essential in

dyad **3** to act as a rectifier. Importantly, they also unambiguously document that rectification in **3** is not due to current flow between the (weakened) DAA donor and the directly attached exTCNQ acceptor moieties.

The monolayer of **3** behaves as a rectifier, since above a threshold voltage the current significantly decreases for negative voltages while at positive voltages the current hardly changes. The rectification ratio RR in dyad **3** (negative current/positive current, RR) is 9 (inset of Figure 8 shows a statistical distribution of the rectification ratio obtained from 180 *I*-*V* curves), which suggests the alignment of dyad **3** to form a well-ordered monolayer[3r] (see BAM and AFM images at 10 $mN \cdot m^{-1}$, Figures S11 and S12, respectively, in the SI). In addition, the RR practically does not decrease after several scans as it has been shown previously in the literature for similar compounds.[3r] The direction of the observed rectification would indicate that the preferred electron current is from the exTCNQ acceptor to the TTF donor.

Conclusions

Two closely related Aviram–Ratner-type molecular dyads comprising TTF as strong donor and DAA-substituted exTCNQ as strong acceptor, separated by the rigid σ-spacer bicyclo[2.2.2]octane (BCO), have been prepared. By installing the acceptor in the final step using the CA–RE cascade, problems such as spontaneous redox chemistry or intramolecular CT from TTF to the acceptor, which had been encountered in previous approaches to molecular rectifying dyads, could be avoided. All electrochemical, optical, and EPR studies in comparison with appropriate reference compounds revealed that there is no significant CT between the TTF moiety and the acceptor moiety exTCNQ in the ground state. Only intramolecular CT between the DAA moiety and the directly connected exTCNQ acceptor part exists in

the ground state. Langmuir-Blodgett monolayer formation was tested for the *n*-butyl- (**2**) and the *n*-octyl- (**3**) substituted TTF-exTCNQ dyads as well as *n*-octyl reference compound **10**. Dyad **3** and reference **10** indeed both formed homogeneous LB films. Gratifyingly, rectification behavior with a rectification ratio (RR) of 9 was observed for dyad **3** due to its proposed charge-separated state under applied voltage. On the other hand, reference **10** did not exhibit an asymmetric *I*-*V* curve but instead showed a symmetric curve, demonstrating the crucial role of the insulated TTF donor moiety in **3**, besides the exTCNQ acceptor moiety for rectification. This result fully validates the rectification proposal by Aviram and Ratner and demonstrates the essential nature of the rigid σ-spacer in **3**. Practical applicability of this system may be possible given the fact that **3** has high thermal and reversible electrochemical stability, which are necessary for an organic molecular rectifier. Synthesis of dyads with even lower HOMO-LUMO gaps based on strong acceptor such as F_4-TCNQ ($E_{red,1}$ = +0.16 V in CH_2Cl_2 *vs.* Fc^+/Fc; TCNQ: $E_{red,1}$ = –0.25 V in CH_2Cl_2 *vs.* Fc^+/Fc) is in progress.

Experimental Section

Materials and methods: Chemicals were purchased from Acros, Aldrich, Fluka, and TCI, and used as received. CH_2Cl_2 was freshly distilled from CaH_2 under nitrogen atmosphere. Column chromatography (CC) and plug filtrations were carried out with SiO_2 60 (particle size 0.040–0.063 mm, 230–400 mesh; Aldrich) or with neutral Al_2O_3 (Brockmann activity I). Thin layer chromatography (TLC) was performed using aluminum sheets coated with 0.2 mm Merck silica gel or < 60 mm Aldrich neutral Al_2O_3. The compounds were visualized by UV light (254 nm) or by visual color change without staining with a colorizing agent. Melting points (m.p.) were measured in open capillaries with a Büchi melting point B540 apparatus and are

uncorrected. “Decomp” refers to decomposition. ^{1}H NMR and ^{13}C NMR spectra were measured on a Bruker DRX 400 MHz, a Bruker AV 400 MHz or Avance II 600 MHz at 25 °C. Chemical shifts (δ) are reported in ppm downfield from $SiMe_4$, with the residual solvent signal as an internal reference. Coupling constants (J) are given in Hz. The apparent resonance multiplicity is described as s (singlet), d (doublet), dd (doublet of doublet), quint. (quintet), hex. (hextet), and m (multiplet). Infrared spectra (IR) were recorded on a Perkin-Elmer BX FT-IR spectrometer; signal designations: s (strong), m (medium), w (weak). Selected absorption bands are reported in wavenumbers (cm^{-1}). UV/Vis spectra were recorded on a Varian CARY-500 spectrophotometer. The spectra were measured in a quartz cuvette of 1 cm at 298 K. The absorption maxima (λ_{max}) are reported in nm with the extinction coefficient (ε) in $M^{-1}cm^{-1}$ in brackets. Shoulders are indicated as sh. High-resolution (HR) ESI-TOF spectra were measured on a Bruker maXis ESI-Q-TOF spectrometer. HR FT-ICR-MALDI spectra were measured on IonSpecUltima Fourier transform (FT) instrument with 3-hydroxypicolinic acid (3-HPA) and 2-[(2E)-3-(4-tert-butylphenyl)-2-methylprop-2-enylidene] malononitrile (DCTB) in THF. The most important signals are reported in m/z units with M^+ as the molecular ion. Size exclusion chromatography (GPC) was performed with BIO-RAD Beads S-X3 as stationary phase and distilled technical solvents at ambient pressure and temperature.

Continuous wave (CW) EPR: The experiment was performed at a frequency of 9.8756 GHz with a Bruker ElexSys E500 spectrometer equipped with a Bruker super high Q resonator ER4122SHQ at ambient temperature. The sample was placed into a thin glass capillary (~0.4 mm inner diameter, BLAUBRAND® micropipettes), and the EPR spectrum was recorded with 100 kHz field modulation, 20 dB attenuation (2

mW incident microwave power), 0.2 mT modulation amplitude, 5.12 ms time constant, and 20.48 ms conversion time.

Preparation and characterization of cast films and LB monolayers incorporating dyads 2 and 3 and reference compound 10: The compounds were assembled by the Langmuir-Blodgett (LB) technique using a Nima Teflon trough with dimensions 720x100 mm^2 housed in a constant temperature (20 ± 1 ºC) clean room. The surface pressure (π) was measured by using a Wilhelmy paper plate pressure sensor, and ultrapure Milli-Q water (resistivity 18.2 MΩcm) was used as subphase. Solutions of **2**, **3**, and **10** ($5 \cdot 10^{-6}$ M) were prepared in chloroform (HPLC grade, 99.9% purchased from Sigma) and spread using a Hamilton micro-syringe held very close to the aqueous surface, allowing the surface pressure to return to a value as close as possible to zero between each addition. The spreading solvent was allowed to completely evaporate over a period of at least 15 min before compression of the Langmuir (L) film at a constant sweeping speed of 0.02 $nm^2 \cdot molecule^{-1} \cdot min^{-1}$. The films were deposited at a constant surface pressure by the vertical dipping method with a dipping speed of 0.6 $cm \cdot min^{-1}$. All the films were transferred by the withdrawal of the substrate from the water subphase for which the transfer ratio is close to 1. Deposition of the films by immersion of the substrates into the water surface resulted in a poor transfer ratio (<0.2). The solid substrates used to support the LB films were quartz, mica, and gold. Gold substrates were purchased from Arrandee®, Schroeer, Germany and were flame-annealed at approximately 800–1000 ºC with a Bunsen burner immediately prior to use to prepare atomically flat Au(111) terraces.[20] Cast films were prepared by spreading a drop of a very diluted solution ($5 \cdot 10^{-6}$ M) onto quartz and gold substrates. The solvent was then allowed to evaporate. These films were

prepared with the purpose of comparison with LB films. UV/Vis spectra were recorded using a normal incident angle with respect to the film plane. X-ray photoelectron spectroscopy (XPS) spectra were acquired on a Kratos AXIS ultra DLD spectrometer with a monochromatic Al Kα X-ray source (1486.6 eV) using a pass energy of 20 eV. To provide a precise energy calibration, the XPS binding energies were referenced to the C1s peak at 284.6 eV. Atomic force microscopy (AFM) experiments were performed by means of a Multimode 8 AFM system from Veeco, using the tapping mode in ambient air conditions. The data were collected with a silicon cantilever provided by Bruker, with a force constant of 40 mN and operating at a resonant frequency of 300 kHz.

Electrical properties of the LB films of dyad 3 and reference compound 10: The electrical properties were recorded with a conductive-AFM (Bruker ICON) under humidity control, ca. 30%, with a N_2 flow using the Peak Force Tunneling AFM (PF-TUNA™) mode, and employing a PF-TUNA™ cantilever from Bruker (coated with Pt/Ir 20 nm, ca. 25 nm radius, 0.4 $N \cdot m^{-1}$ spring constant and 70 kHz resonance frequency). The PF-TUNA™ operation mode for the AFM was chosen in order to avoid lateral forces during the images that would have damaged tip coating and sample surface, while at the same time allowing the use of cantilevers with low spring constant. Thus, this is a method for the conductivity mapping of soft or fragile samples and as such it has been chosen for rectification probing of our LB films, rather than using STM or conducting AFM in conventional contact mode. The peak force tunneling AFM used here combines “tapping” mode AFM with a conducting AFM tip and low-noise current amplifier to probe current flow through the LB film. To be sure that a reasonable contact between the tip and the LB film is obtained without damaging the monolayer a peak force set-point of 65 nN for dyad **3** and 22

nN for compound **10** was applied. Using this peak force set-point, current-voltage (*I-V*) curves were then recorded with the AFM probe placed on top of the LB film and a bias between the substrate and the tip was applied. *I-V* characteristics were recorded by sweeping the tip voltage (±1.6 V) with the LB-coated Au substrate held at ground. To ensure reproducibility and reliability of the results, the *I-V* curves were averaged from multiple scans.

Synthesis: Only the synthesis of dyad **3** is described in this Experimental Section. All other preparations and characterizations are in the Supporting Information.

***N*,*N*-Dioctyl-4-(2-{4-[2-(trimethylsilyl)ethynyl]bicyclo[2.2.2]oct-1-yl}ethynyl)aniline (5)**. A solution of **4**[8] (50 mg, 0.32 mmol) in Et_2O (3 mL) under nitrogen was cooled to –78 °C, treated with 1.6 M *n*-BuLi in hexane (0.25 mL, 0.39 mmol), stirred for 1 h, treated with Me_3SiCl (0.06 mL, 0.47 mmol), and stirred for 1 h at –78 °C and for 1 h at 25 °C. The mixture was diluted with saturated NH_4Cl solution and extracted with Et_2O. Evaporation afforded a colorless solid, which was directly used for the Sonogashira coupling reaction. A solution of the solid residue in Et_3N (5 mL) was purged with nitrogen for 15 min and added to a mixture of *N*,*N*-dioctyl-4-iodoaniline[9] (**2S**, 350 mg, 0.79 mmol), $[PdCl_2(PPh_3)_2]$ (7 mg, 9.6 μmol), and CuI (2.5 mg, 13 μmol) in C_6H_6 (4 mL). The mixture was stirred for 15 h at 25 °C, diluted with Et_2O (20 mL), and filtered through a plug of SiO_2. Evaporation and CC (SiO_2; hexane/CH_2Cl_2 1:0 → 9:1) afforded **5** (60 mg, 35%) as a colorless liquid besides two side-products [4,4'-(bicyclo[2.2.2]octane-1,4-diyl)diethyne-2,1-diyl)bis(*N*,*N*-dioctylaniline (**4S**), colorless liquid (17 mg, 7%), and 1,4-bis(trimethylsilylethynyl)bicyclo[2.2.2]octane (**5S**),[21] colorless solid (17 mg, 15%); see Scheme S1 and Section A in the SI).

Data of **5**: R_f = 0.48 (SiO_2; hexane/CH_2Cl_2 8:2); ^{1}H NMR (400 MHz, $CDCl_3$, 298 K; assignment based on DQF-COSY, HSQC, and HMBC spectra): δ = 0.13 (s, 9 H; $Si(CH_3)_3$), 0.87 – 0.91 (m, 6 H; 2 CH_3), 1.26 – 1.31 (m, 20 H; 2 (CH_2)$_5CH_3$), 1.49 – 1.59 (m, 4 H; $N(CH_2CH_2)_2$), 1.77 – 1.83 (m, 12 H; $C(CH_2CH_2)_3C$), 3.23 (t, J = 7.7 Hz, 4 H; $N(CH_2)_2$), 6.49 (d, J = 9.0 Hz, 2 H; H–C(2,6)), 7.18 ppm (d, J = 8.8 Hz, 2 H; H–C(3,5)); ^{13}C NMR (100 MHz, $CDCl_3$, 298 K; assignment based on DQF-COSY, HSQC, and HMBC spectra): δ = 0.45 ($Si(CH_3)_3$), 14.24 (2 CH_3), 22.79 (2 CH_2CH_3), 26.86 and 27.09 (C(1',4')), 27.28, 27.34, 29.45, 29.62, and 31.97 (2 (CH_2)$_5CH_2CH_3$), 32.08 and 32.18 ($C(CH_2CH_2)_3C$), 51.09 ($N(CH_2)_2$), 81.31 (C≡C–C(4)), 83.68 (C≡C–Si), 93.63 (C≡C–C(4)), 109.71 (C(4)), 111.37 (C(2,6)), 114.36 ((C≡C–Si), 132.77 (C(3,5)), 147.56 ppm (C(1)); IR (ATR): $\tilde{\eta}$ = 2953 (m), 2924 (s), 2854 (m), 2109 (w), 1608 (s), 1517 (s), 1465 (w), 1456 (w), 1398 (w), 1369 (m), 1274 (w), 1191 (w), 1119 (w), 811 (m), 765 (w), 750 cm^{-1} (w); HR-ESI-MS: *m/z* (%): 546.4487 (100, $[M + H]^+$, calcd for $C_{37}H_{60}NSi^+$: 546.4490).

4-[2-(4-Ethynylbicyclo[2.2.2]oct-1-yl)ethynyl]-*N*,*N*-dioctylaniline (6): A solution of **5** (50 mg, 92 μmol) in MeOH (5 mL), was treated with K_2CO_3 (129 mg, 0.93 mmol), stirred at room temperature for 2.5 h, diluted with H_2O (50 mL), and extracted with CH_2Cl_2 (2×50 mL). Evaporation gave **6** (42 mg, 98%) as a colorless liquid. R_f = 0.60 (Al_2O_3; pentane/CH_2Cl_2 9:1); ^{1}H NMR (400 MHz, $CDCl_3$, 298 K; assignment based on DQF-COSY, HSQC, and HMBC spectra): δ = 0.89 (t, J = 6.8 Hz, 6 H; 2 CH_3), 1.24 – 1.32 (m, 20 H; 2 (CH_2)$_5CH_3$), 1.50 – 1.57 (m, 4 H; $N(CH_2CH_2)_2$), 1.79 – 1.86 (m, 12 H; $C(CH_2CH_2)_3C$), 2.09 (s, 1 H; C≡CH), 3.22 (t, J = 8.0 Hz, 4 H; ($N(CH_2)_2$), 6.49 (d, J = 8.8 Hz, 2 H; H–C(2,6)), 7.18 ppm (d, J = 8.7 Hz, 2 H; H–C(3,5)); ^{13}C NMR (100 MHz, $CDCl_3$, 298 K; assignment based on DQF-COSY,

HSQC, and HMBC spectra): δ = 14.24 (2 CH_3), 22.79 (2 CH_2CH_3), 26.27 and 26.84 ($C(CH_2CH_2)_3C$), 27.27, 27.33, 29.45, 29.62, 31.97 (2 $(CH_2)_5CH_2CH_3$), 32.03 and 32.11 ($C(CH_2CH_2)_3C$), 51.09 ($N(CH_2)_2$), 68.08 (C≡CH), 81.39 (C≡C–C(4)), 91.62 (C≡CH), 93.44 (C≡C–C(4)), 109.60 (C(4)), 111.36 (C(2,6)), 132.77 (C(3,5)), 147.58 ppm (C(1)); IR (ATR): $\tilde{\nu}$ = 3311 (w), 2922 (s), 2856 (s), 2109 (w), 1608 (s), 1517 (s), 1465 (m), 1455 (m), 1369 (m), 1340 (m), 1276 (m), 1239 (m), 1190 (m), 1130 (m), 1107 (s), 1061 (m), 953 (w), 842 (w), 811 (m), 763 (w), 750 (w), 721 (w), 626 cm^{-1} (m); HR-ESI-MS: *m/z* (%): 474.4089 (100, $[M + H]^+$, calcd for $C_{34}H_{52}N_2^+$: 474.4094).

***N,N*-Dioctyl-4-[(4-{[2-(1,3-dithiol-2-ylidene)]-1,3-dithiol-4-yl]ethynyl}bicyclo[2.2.2]oct-1-yl)ethynyl]aniline (7)**: A solution of **6** (42 mg, 89 μmol) in Et_3N (3 mL) was purged with nitrogen for 10 min and added to a suspension of 4-iodo-TTF[10] (**3S**, 58 mg, 180 μmol), $[Pd(PPh_3)_4]$ (10 mg, 9 μmol), and CuI (3.5 mg, 18 μmol) in C_6H_6 (2 mL). The mixture was stirred for 15 h at 60 °C, cooled to room temperature, diluted with water (20 mL), and extracted with Et_2O (3×20 mL). Evaporation and CC (Al_2O_3; pentane/CH_2Cl_2 1:0 → 9:1) afforded **7** (24 mg, 40%) as a yellow liquid. R_f = 0.25 (Al_2O_3; pentane/CH_2Cl_2 9:1); ^{1}H NMR (400 MHz, C_6D_6, 298 K; assignment based on DQF-COSY, HSQC, and HMBC spectra): δ = 0.91 (t, *J* = 7.0 Hz, 6 H; 2 CH_3), 1.09 – 1.32 (m, 20 H; 2 $(CH_2)_5CH_3$), 1.39 – 1.47 (m, 4 H; $N(CH_2CH_2)_2$), 1.59 – 1.63 (m, 6 H; C(4')$(CH_2CH_2)_3$C(1')), 1.77 – 1.81 (m, 6 H; C(4')$(CH_2CH_2)_3$C(1')), 3.02 (br. t, *J* ≈ 7.6 Hz, 4 H; $N(CH_2)_2$), 5.38 (s, 2 H; H–C(4''',5''')), 5.73 (s, 1 H; H–C(5'')), 6.56 (d, *J* = 9.0 Hz, 2 H; H–C(2,6)), 7.55 ppm (d, *J* = 8.9 Hz, 2 H; H–C(3,5)); ^{13}C NMR (100 MHz, C_6D_6, 298 K; assignment based on DQF-COSY, HSQC, and HMBC spectra): δ = 14.38 (2 CH_3), 23.09 (2 CH_2CH_3), 27.17 (C(1')), 27.38 (C(4')), 27.44, 27.63, 29.74, 29.88, and 32.30 (2 $(CH_2)_5CH_2CH_3$),

31.77 (C(4')(CH_2CH_2)$_3$C(1')), 32.24 (C(4')(CH_2CH_2)$_3$C(1')), 51.14 (N(CH_2)$_2$), 72.72 (C≡C–C(4'')), 82.48 (C≡C–C(4')), 93.67 (C≡C–C(4')), 101.60 (C≡C–C(4'')), 108.83 (C(2''')), 110.98 (C(4)), 111.95 (C(2,6)), 112.93 (C(2'')), 116.82 (C(4'')), 118.67 and 119.07 (C(4''',5''')), 123.14 (C(5'')), 133.35 (C(3,5)), 147.93 ppm (C(1)); IR (ATR): $\tilde{n}$= 2951 (m), 2922 (s), 2853 (m), 2213 (w), 1607 (s), 1516 (s), 1465 (w), 1455 (m), 1398 (w), 1368 (m), 1275 (w), 1263 (w), 1213 (w), 1189 (m), 1107 (w), 952 (w), 860 (w), 812 (s), 796 (m), 777 (m), 738 (m), 640 cm^{-1} (m); HR-MALDI/ESI (dual)-MS: *m*/*z* (%): 675.3056 (100, M^+, calcd for $C_{40}H_{53}NS_4^+$: 675.3055).

2-[2-[4-(Dioctylamino)phenyl]-2-[4-(dicyanomethylene)cyclohexa-2,5-dien-1-ylidene]-1-(4-{2-[2-(1,3-dithiol-2-ylidene)-1,3-dithiol-4-yl]ethynyl}bicyclo[2.2.2]oct-1-yl)ethylidene]-malonodinitrile (3). A solution of **7** (64 mg, 95 μmol) and TCNQ (19 mg, 95 μmol) in 1,1,2,2-tetrachloroethane (30 mL) was stirred for 2.5 h at 120 °C. Evaporation and CC (pentane/CH_2Cl_2 4:1 → 1:2) gave **3** (62 mg, 75%) as a maroon metallic solid (green in CH_2Cl_2 solution). R_f = 0.60 (Al_2O_3; pentane/CH_2Cl_2 3:7); m.p. 109 – 110 °C (no decomp); ^{1}H NMR (400 MHz, C_6D_6, 298 K; assignment based on DQF-COSY, HSQC, HMBC, and NOESY spectra): δ = 0.93 (t, *J* = 6.7 Hz, 6 H; 2 CH_3), 1.19 – 1.34 (m, 20 H; 2 (C*H*$_2$)$_5$CH$_3$), 1.38 – 1.50 (m, 10 H; N(CH_2C*H*$_2$)$_2$, C(4')(CH_2C*H*$_2$)$_3$C(1')), 1.62 – 1.65 (m, 6 H; C(4')(C*H*$_2$CH$_2$)$_3$C(1')), 3.05 (br. t, *J* ≈ 8.0 Hz, 4 H; N(CH_2)$_2$), 5.39 (s, 2 H; H–C(4''',5''')), 5.75 (s, 1 H; H–C(5'')), 6.28 (dd, *J* = 9.5, 1.9 Hz, 1 H; H–C(6''''')), 6.53 (d, *J* = 8.5 Hz, 2 H; H–C(3'''',5'''')), 6.80 (dd, *J* = 9.6, 2.0 Hz, 1 H; H–C(2''''')), 6.88 – 6.92 ppm (m, 4 H; H–C(2'''',6'''',3''''',5''''')); ^{13}C NMR (100 MHz, C_6D_6, 298 K; assignment based on DQF-COSY, HSQC, and HMBC spectra): δ = 14.35 (2 CH_3), 23.07 (2 *C*H$_2$CH$_3$), 27.39 (C(4')), 27.49, 27.62, 29.71, 29.73, and

29.82 (2 (CH_2)$_5$$CH_2$$CH_3$), 31.15 (C(4')($CH_2CH_2$)$_3$C(1')), 32.19 (C(4')($CH_2CH_2$)$_3$C(1')), 40.36 (C(1')), 51.38 (N(CH_2)$_2$), 73.26 (C(4'')–*C*≡C), 73.44 (C(4'''''')=*C*(CN)$_2$), 90.53 (C(2)), 99.68 (C(4'')–C≡*C*), 108.19 (C(2''')), 112.33 (C(3'''',5'''')), 112.59 (C(2'')), 112.80 (C≡N), 113.68 (C(4'')), 114.82 (C≡N), 114.90 (C≡N), 116.24 (C≡N), 118.77 and 119.04 (C(4''',5''')), 119.89 (C(1'''')), 123.92 (C(5'')), 125.31 and 125.34 (C(3''''',5''''')), 129.95 (C(1''''')), 133.53 (C(6''''')), 134.00 (C(2'''',6'''')), 134.75 (C(2''''')), 151.19 (C(4''''')), 152.15 (C(4'''')), 154.23 (*C*–C=C(2)), 186.47 ppm (*C*=C(2)); IR (ATR): $\tilde{n}$ = 3075 (w), 2921 (s), 2853 (m), 2213 (w), 1607 (s), 1517 (s), 1465 (m), 1455 (m), 1398 (w), 1368 (m), 1271 (w), 1214 (w), 1188 (m), 1107 (w), 952 (w), 859 (w), 812 (m), 796 (m), 777 (m), 755 (w), 736 (m), 641 cm^{-1} (m); UV/Vis (CH_2Cl_2): λ_{max} (ε) = 429 (14 500), 669 nm (49 000 M^{-1} cm^{-1}); HR-MALDI/ESI (dual)-MS: *m*/*z* (%): 879.3494 (100, M^+, calcd for $C_{52}H_{57}N_5S_4^+$: 879.3491); elemental analysis calcd (%) for $C_{52}H_{57}N_5S_4$ (880.3): C 70.95, H 6.66, N 7.96; found: C 71.43, H 6.66, N 7.72.

Acknowledgements

This work was supported by the ERC Advanced grant no. 246637 ("OPTELOMAC") and the Swiss National Science Foundation (SNF). ADF acknowledges the NSF-IRFP (U.S.A.) for a postdoctoral fellowship. SM and PC are grateful for financial assistance from Ministerio de Ciencia e Innovación from Spain in the framework of grants CTQ2012-33198 and CTQ2013-50187-EXP.We thank Dr. Nils Trapp for help with the X-ray crystal structures, Dr. Antorrena and Dr. González-Orive for their help with the XPS and AFM experiments, respectively.

References

[1] A. Aviram, M. A. Ratner, *Chem. Phys. Lett.* **1974**, *29*, 277–283.

[2] a) R. L. Carroll, C. B. Gorman, *Angew. Chem. Int. Ed.* **2002**, *41*, 4378–4400; *Angew. Chem*. **2002**, *114*, 4556–4579; b) R. M. Metzger, *Chem. Rev.* **2003**, *103*, 3803–3834; c) G. Maruccio, R. Cingolani, R. Rinaldi, *J. Mater. Chem.* **2004**, *14*, 542–554; d) R. M. Metzger, *Synth. Met.* **2009**, *159*, 2277–2281; e) R. M. Metzger, D. L. Mattern, *Top. Curr. Chem.* **2012**, *313*, 39–84.

[3] a) N. J. Geddes, J. R. Sambles, D. J. Jarvis, W. G. Parker, D. J. Sandman, *Appl. Phys. Lett.* **1990**, *56*, 1916–1918; b) G. J. Ashwell, J. R. Sambles, A. S. Martin, W. G. Parker, M. Szablewski, *J. Chem. Soc., Chem. Commun*. **1990**, 1374–1376; c) A. S. Martin, J. R. Sambles, G. J. Ashwell, *Phys. Rev. Lett.* **1993**, *70*, 218–221; d) R. M. Metzger, B. Chen, U. Höpfner, M. V. Lakshmikantham, D. Vuillaume, T. Kawai, X. Wu, H. Tachibana, T. V. Hughes, H. Sakurai, J. W. Baldwin, C. Hosch, M. P. Cava, L. Brehmer, G. J. Ashwell, *J. Am. Chem. Soc.* **1997**, *119*, 10455–10466; e) A. C. Brady, B. Hodder, A. S. Martin, J. R. Sambles, C. P. Ewels, R. Jones, P. R. Briddon, A. M. Musa, C. A. Panetta, D. L. Mattern, *J. Mater. Chem.* **1999**, *9*, 2271–2275; f) R. M. Metzger, *Acc. Chem. Res.* **1999**, *32*, 950–957; g) G. J. Ashwell, D. S. Gandolfo, *J. Mater. Chem.* **2001**, *11*, 246–248; h) T. Xu, I. R. Peterson, M. V. Lakshmikantham, R. M. Metzger, *Angew. Chem. Int. Ed.* **2001**, *40*, 1749–1752; *Angew. Chem.* **2001**, *113*, 1799–1802; i) R. M. Metzger, T. Xu, I. R. Peterson, *J. Phys. Chem. B* **2001**, *105*, 7280–7290; j) G. J. Ashwell, D. S. Gandolfo, *J. Mater. Chem.* **2002**, *12*, 411–415; k) G. J. Ashwell, D. S. Gandolfo, R. Hamilton, *J. Mater. Chem.* **2002**, *12*, 416–420; l) M.-K. Ng, L. Yu, *Angew. Chem. Int. Ed.* **2002**, *41*, 3598–3601; *Angew. Chem.* **2002**, *114*, 3750–3753; m) G. J. Ashwell, R. Hamilton, L. R. H. High, *J. Mater. Chem.* **2003**, *13*, 1501–1503; n) F. C. Krebs, H. Spanggaard, N. Rozlosnik, N. B. Larsen, M.

Jørgensen, *Langmuir* **2003**, *19*, 7873–7880; o) G. J. Ashwell, W. D. Tyrrell, A. J. Whittam, *J. Am. Chem. Soc.* **2004**, *126*, 7102–7110; p) G. J. Ashwell, A. Chwialkowska, L. R. H. High, *J. Mater. Chem.* **2004**, *14*, 2389–2394; q) P. Jiang, G. M. Morales, W. You, L. Yu, *Angew. Chem. Int. Ed.* **2004**, *43*, 4471–4475; *Angew. Chem.* **2004**, *116*, 4571–4575; r) G. Ho, J. R. Heath, M. Kondratenko, D. F. Perepichka, K. Arseneault, M. Pézolet, M. R. Bryce, *Chem. Eur. J.* **2005**, *11*, 2914–2922; s) M. Elbing, R. Ochs, M. Koentopp, M. Fischer, C. von Hänisch, F. Weigend, F. Evers, H. B. Weber, M. Mayor, *Proc. Natl. Acad. Sci. U.S.A.* **2005**, *102*, 8815–8820; t) I. Díez-Pérez, J. Hihath, Y. Lee, L. Yu, L. Adamska, M. A. Kozhushner, I. I. Oleynik, N. Tao, *Nat. Chem.* **2009**, *1*, 635–641; u) A. Batra, P. Darancet, Q. Chen, J. S. Meisner, J. R. .Widawsky, J. B. Neaton, C. Nuckolls, L. Venkataraman, *Nano Lett.* **2013**, *13*, 6233–6237.

[4] D. F. Perepichka, M. R. Bryce, C. Pearson, M. C. Petty, E. J. L. McInnes, J. P. Zhao, *Angew. Chem. Int. Ed.* **2003**, *42*, 4636–4639; *Angew. Chem.* **2003**, *115*, 4784–4787.

[5] D. F. Perepichka, M. R. Bryce, E. J. L. McInnes, J. P. Zhao, *Org. Lett.* **2001**, *3*, 1431–1434.

[6] a) M. Kivala, C. Boudon, J.-P. Gisselbrecht, P. Seiler, M. Gross, F. Diederich, *Chem. Commun.* **2007**, 4731–4733; b) M. Kivala, C. Boudon, J.-P. Gisselbrecht, B. Enko, P. Seiler, I. B. Müller, N. Langer, P. D. Jarowski, G. Gescheidt, F. Diederich, *Chem. Eur. J.* **2009**, *15*, 4111–4123; c) P. Fesser, C. Iacovita, C. Wäckerlin, S. Vijayaraghavan, N. Ballav, K. Howes, J.-P. Gisselbrecht, M. Crobu, C. Boudon, M. Stöhr, T. A. Jung, F. Diederich, *Chem. Eur. J.* **2011**, *17*, 5246–5250; d) L. M. Urner, M. Sekita, N. Trapp, W. B. Schweizer, M. Wörle, J.-P.

Gisselbrecht, C. Boudon, D. M. Guldi, F. Diederich, *Eur. J. Org. Chem.* **2015**, 91–108.

[7] a) K.-i. Onuma, Y. Kai, N. Yasuoka, N. Kasai, *Bull. Chem. Soc. Jpn.* **1975**, *48*, 1696–1700; b) X. Tang, W. Liu, J. Wu, C.-S. Lee, J. You, P. Wang, *J. Org. Chem.* **2010**, *75*, 7273–7278; c) M. I. Bruce, *Aust. J. Chem.* **2011**, *64*, 77–103; d) Y. Washino, T. Michinobu, *Macromol. Rapid Commun.* **2011**, *32*, 644–648; e) Y. Washino, K. Murata, T. Michinobu, *Polym. Bull.* **2012**, *69*, 137–147; f) T. Shoji, J. Higashi, S. Ito, T. Okujima, M. Yasunami, N. Morita, *Org. Biomol. Chem.* **2012**, *10*, 2431–2438; g) M. I. Bruce, A. Burgun, G. Grelaud, C. Lapinte, B. W. Skelton, N. N. Zaitseva, *Aust. J. Chem.* **2012**, *65*, 763–772; h) T. Shoji, E. Shimomura, M. Maruyama, A. Maruyama, S. Ito, T. Okujima, K. Toyota, N. Morita, *Eur. J. Org. Chem.* **2013**, 7785–7799; i) T. Shoji, M. Maruyama, E. Shimomura, A. Maruyama, S. Ito, T. Okujima, K. Toyota, N. Morita, *J. Org. Chem.* **2013**, *78*, 12513–12524.

[8] a) R. H. Goldsmith, J. Vura-Weis, A. M. Scott, S. Borkar, A. Sen, M. A. Ratner, M. R. Wasielewski, *J. Am. Chem. Soc.* **2008**, *130*, 7659–7669; b) C. Lemouchi, C. S. Vogelsberg, L. Zorina, S. Simonov, P. Batail, S. Brown, M. A. Garcia-Garibay, *J. Am. Chem. Soc.* **2011**, *133*, 6371–6379.

[9] W. Huang, H. Chen, *Macromolecules* **2013**, *46*, 2032–2037.

[10] C. Wang, A. Ellern, V. Khodorkovsky, J. Bernstein, J. Y. Becker, *J. Chem. Soc., Chem. Commun.* **1994**, 983–984.

[11] H.-R. Tseng. S. A. Vignon, J. F. Stoddart, *Angew. Chem. Int. Ed.* **2003**, *42*, 1491–1495; *Angew. Chem.* **2003**, *115*, 1529–1533.

[12] S.-i. Kato, M. Kivala, W. B. Schweizer, C. Boudon, J.-P. Gisselbrecht, F. Diederich, *Chem. Eur. J.* **2009**, *15*, 8687–8691.

[13] M. Giffard, P. Alonso, J. Garin, A. Gorgues, T. P. Nguyen, P. Richomme, A. Robert, J. Roncali, S. Uriel, *Adv. Mater.* **1994**, *6*, 298–300.

[14] B. Breiten, M. Jordan, D. Taura, M. Zalibera, M. Griesser, D. Confortin, C. Boudon, J.-P. Gisselbrecht, W. B. Schweizer, G. Gescheidt, F. Diederich, *J. Org. Chem.* **2013**, *78*, 1760–1767.

[15] M. J. Frisch, G. W. Trucks, H. B. Schlegel, G. E. Scuseria, M. A. Robb, J. R. Cheeseman, G. Scalmani, V. Barone, B. Mennucci, G. A. Petersson, H. Nakatsuji, M. Caricato, X. Li, H. P. Hratchian, A. F. Izmaylov, J. Bloino, G. Zheng, J. L. Sonnenberg, M. Hada, M. Ehara, K. Toyota, R. Fukuda, J. Hasegawa, M. Ishida, T. Nakajima, Y. Honda, O. Kitao, H. Nakai, T. Vreven, J. A. Montgomery, Jr., J. E. Peralta, F. Ogliaro, M. Bearpark, J. J. Heyd, E. Brothers, K. N. Kudin, V. N. Staroverov, R. Kobayshi, J. Normand, K. Raghavachari, A. Rendell, J. C. Burant, S. S. Iyengar, J. Tomasi, M. Cossi, N. Rega, J. M. Millam, M. Klene, J. E. Knox, J. B. Cross, V. Bakken, C. Adamo, J. Jaramillo, R. Gomperts, R. E. Stratmann, O. Yazyev, A. J. Austin, R. Cammi, C. Pomelli, J. W. Ochterski, R. L. Martin, K. Morokuma, V. G. Zakrzewski, G. A. Voth, P. Salvador, J. J. Dannenberg, S. Dapprich, A. D. Daniels, Ö. Farkas, J. B. Foresman, J. V. Ortiz, J. Cioslowski, and D. J. Fox, *Gaussian 09*, Revision A.1, Gaussian, Inc., Wallingford CT, **2009**.

[16] a) G. Roberts, *Langmuir-Blodgett Films*, Plenum Press, New York, **1990**; b) M. R. Bryce, M. C. Petty, *Nature* **1995**, *374*, 771–776; c) *Introduction to Molecular Electronics* (Eds. M. C. Petty, M. R. Bryce, D. D. Bloor), Oxford University Press, New York, **1995**.

[17] a) M. Haro, B. Giner, C. Lafuente, M. C. López, F. M. Royo, P. Cea, *Langmuir* **2005**, *21*, 2796–280; b) A. Villares, D. P. Lydon, P. J. Low, B. J. Robinson, G. J. Ashwell, F. M. Royo, P. Cea, *Chem. Mater.* **2008**, *20*, 258–264.

[18] S. Zhou, Y. Liu, W. Qiu, Y. Xu, X. Huang, Y. Li, L. Jiang, D. Zhu, *Adv. Funct. Mater*. **2002**, *12*, 65–69.

[19] a) H. M. Osorio, P. Cea, L. M. Ballesteros, I. Gascón, S. Marqués-González, R. J. Nichols, F. Pérez-Murano, P. J. Low, S. Martín, *J. Mater. Chem. C* **2014**, *2*, 7348–7355; b) L. M. Ballesteros, S. Martín, J. Cortés, S. Marqués-González, F. Pérez-Murano, R. J. Nichols, P. J. Low, P. Cea, *Adv. Mater. Interfaces* **2014**, *1*, 1400128.

[20] W. Haiss, D. Lackey, J. K. Sass, K. H. Besocke, *J. Chem. Phys.* **1991**, *95*, 2193–2196.

[21] Lemouchi, C.; Barrès, A.-L.; Mézière, C.; Rondeau, D.; Zorina, L.; Wzietek, P.; Batail, P. *Dalton Trans.* **2011**, *40*, 8075–8078.

Table of Content Text and Figure

Design and Synthesis of Aviram-Ratner-Type Dyads and Rectification Studies in Langmuir-Blodgett (LB) Films

Govindasamy Jayamurugan, Vijayendran Gowri, David Hernández, Santiago Martin, Cagatay Dengiz, Francesc Pérez-Murano, Jean-Paul Gisselbrecht, Corinne Boudon, W. Bernd Schweizer, Benjamin Breiten, Aaron D. Finke, Gunnar Jeschke, Bruno Bernet, Laurent Ruhlmann, Pilar Cea,* and François Diederich*

A molecular dyad, closely resembling the original design by Aviram and Ratner, featuring a strong donor (TTF), separated by a rigid insulating σ-spacer from a strong extended TCNQ acceptor (exTCNQ), has been designed, synthesized, and fully characterized. Langmuir-Blodgett films were prepared and showed the asymmetric current-voltage (*I*-*V*) curve characteristic for rectification, wereas a control compound lacking the TTF donor showed a symmetric *I*-*V* curve.